Isolation, Size Estimates, and Spectral Heterogeneity of an Oligomeric Series of Light-Harvesting 1 Complexes from *Rhodobacter sphaeroides*†

Willem H. J. Westerhuis,‡,§ James N. Sturgis,|| Emma C. Ratcliffe,⊥ C. Neil Hunter,⊥ and Robert A. Niederman*,‡

Department of Molecular Biology and Biochemistry, Rutgers University, Piscataway, New Jersey 08854-8082 USA, Laboratoire d'Ingénierie des Systèmes Macromoléculaires, Institut de Biologie Structurale et Microbiologie, CNRS, 31 Chemin Joseph Aiguier, 13402 Marseilles Cedex 20, France, and Department of Molecular Biology and Biotechnology, University of Sheffield, Sheffield S10 2TN, United Kingdom

Received August 14, 2001; Revised Manuscript Received April 29, 2002

ABSTRACT: A series of light-harvesting 1 (LH1) complexes was isolated by lithium dodecyl sulfate−polyacrylamide gel electrophoresis at 4 °C from *Rhodobacter sphaeroides* M21, which lacks the peripheral light-harvesting 2 (LH2) complex. This ladder of LH1 bands was also demonstrated in the wild type, partially superimposed upon a smaller number of LH2 complexes. An assessment of electrophoretic mobility vs acrylamide concentration, in which the reaction center LM particle and annular LH1 and LH2 complexes were used as standards of known structure, indicated that the LH1 gel bands 2 to 10 represent regular oligomers of an $\alpha\beta$ heterodimeric unit, that vary in size from $(\alpha\beta)_{2-3}$ to $(\alpha\beta)_{10-11}$. The isolated LH1 complexes exhibited oligomeric state dependent optical properties, characterized by red shifts in near-IR absorption and emission maxima at 77 K of ∼6 nm as aggregate sizes increased from ∼3 to 7−8 $\alpha\beta$-heterodimers, accompanied by shifts in highly polarized fluorescence from the blue to the red side of the absorption band. This has been explained by the oligomerization of heterodimers to form a curvilinear array of excitonically coupled chromophores, with the anisotropic long-wavelength component, designated originally as B896, corresponding to low energy excitonic transitions arising from interactions within inhomogeneous BChl clusters [Westerhuis et al. (1999) *J. Phys. Chem. B 103*, 7733−7742]. Differences in electrophoretic profiles of LH1 bands between strains M21 and M2192, an LH1-only strain that also lacks PufX, further suggested that the more rapidly migrating bands represent arced fragments of the curvilinear array of LH1 complexes thought to exist as a large closed circular structure only in the latter strain. The electrophoretic banding pattern also indicated that the LH1 complex may be located at the peripheries of dimeric intramembrane particle arrays seen in freeze-fracture replicas of tubular M21 membranes; the possible role for the PufX protein in the assembly of these structures is discussed.

The photosynthetic units of the proteobacterium *Rhodobacter sphaeroides* contain two integral membrane light-harvesting complexes, designated as LH1[1] and LH2, that function as core and peripheral antennae, respectively. Radiant energy harvested by LH2 is transferred to LH1, which directs these excitations to the photosynthetic reaction center, where they are used to produce a transmembrane charge separation (*1*). The apoproteins of both LH complexes consist of heterodimers of α- and β-polypeptides containing ∼50−60 amino acid residues (*2*, *3*), which in LH1, bind two molecules each of BChl and carotenoid (*4*), and in LH2, two B850 BChls, one B800 BChl, and one to two carotenoids (*5*, *6*). The α- and β-polypeptides are highly homologous among a large number of photosynthetic bacteria (*7*), and share a common tripartite structure thought to consist of a single transmembrane α-helix separating N- and C-terminal domains of varying length at the cytoplasmic and periplasmic surfaces of the ICM, respectively.

These predicted structural features have been established by the atomic-resolution structure of the LH2 complex from the related bacterium *Rhodopseudomonas acidophila* determined by X-ray crystallography (*8*). The circular arrangement of 18 alternating α- and β-B850 BChls with overlapping bacteriochlorin moieties, sandwiched between two concentric cylinders of transmembrane helices, constitutes an annulus for rapid delocalization of excitations, allowing energy transfer both within the same LH2 ring and to adjacent rings (*9*). A similar structure, but with eight rather than nine α- and β-units, has been determined for the crystalline LH2

† This work was supported by U.S. Department of Agriculture Grant 91-01640, National Science Foundation Grants DMB85-12587 and MCB90-19570 and Biomedical Research Support grant PHS RR 07058-22 (R.A.N.). W.H.J.W. was the recipient of fellowships from the Charles and Johanna Busch Memorial Fund Award and the European Community Human Capital and Mobility Programme. E.C.R. is supported by a Ph.D. studentship from the BBSRC (U.K.).

* To whom correspondence should be addressed. Phone: (732) 445-3985 Fax: (732) 445-4213. E-mail: rniederm@rci.rutgers.edu.

§ Present address: Twinsoft, Havenweg 24a, Postbus 76, 4130 EB Vianen, The Netherlands.

‡ Rutgers University.

|| Institut de Biologie Structurale et Microbiologie.

⊥ University of Sheffield.

[1] Abbreviations: BChl, bacteriochlorophyll *a*; ICM, intracytoplasmic membrane; LDS, lithium dodecyl sulfate; LH1, core light-harvesting complex with near-IR absorbance maximum at B875 nm; LH2, peripheral light-harvesting complex with near-IR absorbance maxima at 800 and 850 nm; OG, *n*-octyl-β-D-glucopyranoside; PAGE, polyacrylamide gel electrophoresis.

10.1021/bi011663b CCC: $22.00
Published on Web 06/11/2002

complex of *Phaeospirillum molischianum* (*10*), while in *R. sphaeroides*, the LH2 complex consists of an $(\alpha\beta)_9$ ring (*11*), as in *Rp. acidophila.* Recent topographs obtained by atomic force microscopy also revealed a nonameric organization within the LH2 complex of *Rubrivivax gelatinosus* (*12*). Cryoelectron microscopy and image processing (*13*) suggest that the LH1 complex of *Rhodospirillum rubrum* also forms a ring-like assembly composed of 16 $\alpha\beta$ units. A similar arrangement is also likely for the LH1 complex of *R. sphaeroides*, based upon an analysis of negatively stained two-dimensional crystals of LH1 and LH1-reaction center complexes of a strain lacking the PufX protein (*11*), but closed LH1 rings do not normally appear to be formed in this organism (*14*). In addition, a solution structure has been determined for the *R. sphaeroides* LH1β polypeptide by homonuclear NMR spectroscopy (*15*), which suggests that besides a transmembrane α-helix, a second, N-terminal α-helix is present that forms an acute angle to the membrane plane. This basic helix−hinge−helix structure has been largely confirmed for the LH1β polypeptide bound to BChl *a* in detergent micelles by a recent multidimensional NMR study that showed the amphipathic N-terminal helix embedded in the micelle surface (*16*).

With these significant advances as a structural framework, it is now possible to gain a more highly detailed understanding of the assembly, organization, optical properties, and excitation energy transfer mechanisms of bacterial light-harvesting complexes. Important functional questions include how their absorbance behavior is modulated to facilitate efficient energy migration downhill to the reaction center, and the extent to which excitons are delocalized over the ring of antenna BChls. However, it is not clear whether complete rings of LH1 normally exist in vivo. The suggestion that the PufX polypeptide interrupts the ring (*17*) derives support from a recent electron microscopy projection map of negatively stained tubular membranes from an LH2$^-$ *R. sphaeroides* strain (*14*), in which regular arrays of "C"-shaped structures are observed that were proposed to represent the LH1 complex. Estimates of LH1-reaction center stoichiometry suggest an LH1 complex consists of 12−14 $\alpha\beta$ units in the presence of PufX (*18*), as opposed to the $(\alpha\beta)_{16}$ complex implied for a complete ring (*13*). Moreover, recent linear dichroism measurements showed that the presence of PufX confers a long-range order upon LH1-reaction center arrays within LH2$^-$ membranes that does not exist in its absence (*19*).

It is clear that PufX plays an important role in the organization and function of the LH1-reaction center complex. Here, we show that a gentle method for the isolation of a well-defined series of oligomeric LH1 complexes with systematic variations in their aggregation state-dependent spectroscopic properties, proceeds more readily in the presence of PufX. Ten distinct LH1 bands are isolated from the LH2$^-$ *R. sphaeroides* mutant strain M21 by this procedure, in which membranes are solubilized with LDS and subjected to nondenaturing PAGE at 4 °C. The electrophoretic migration behavior of these oligomers is analyzed in the light of the current structural information available for the LH1 antenna. The resulting estimates showed that the LH1 aggregates represent a well-defined series of oligomers, gradually increasing in size from $(\alpha\beta)_{2-3}$ to $(\alpha\beta)_{10-11}$, with the consecutive gel bands differing by a mass approximating that of a single $\alpha\beta$-heterodimer. In addition, their fluorescence polarization properties (*20*) are compared to those of LH1 complexes of reduced size from mutant strains with truncations at the C-terminus of the α-polypeptide (*21*). We also present ultrastructural evidence for the presence of highly ordered arrays of dimeric complexes in the tubular membranes of mutant M21.

MATERIALS AND METHODS

Strains, Growth Methods, and Membrane Isolation. The strains used in this study included *R. sphaeroides* wild-type NCIB 8253 and several mutants derived from this strain: NF57, which lacks the LH1 and reaction center complexes (*22*); M21, which lacks the LH2 complex (*22*); and M2192, a reaction center-less derivative of M21 (*23*). Mutants NF57 and M21 were isolated following mutagenesis of wild-type strain NCIB 8253 with *N*-methyl-*N*′-nitro-*N*-nitrosoguanidine (*22*). Both the missing complexes and photosynthetic competence were restored to strain NF57 by complementation with plasmid pSCN5H-1 which contains the *puh*A structural gene encoding the H subunit of the reaction center (*24*). The LH2 complex, as well as the ability to form vesicular rather than tubular ICM (see Supporting Information), was restored to strain M21 by complementation with plasmid pMA81 containing the *puc*BA structural genes encoding the respective LH2-β and LH2-α polypeptides (*22*). Strain M2192 was derived from strain M21 after insertion of transposon Tn5 into the *puf*L gene encoding the L subunit of the reaction center (*23*). In this strain, it proved difficult to observe any internal membrane, and most of the cytoplasmic membrane was closely apposed to the outer membrane (see Supporting Information). Reaction center activity was reestablished in M2192 by complementation with plasmid pSRC2 containing the *puf*LM genes; pufM encodes the M subunit of the reaction center.

All strains were grown on M22+ medium (*25*); strains NF57, M21, and M2192 were grown semiaerobically (*5*). In addition, the wild type and strain M21 were grown photoheterotrophically at low light intensity (*26*). Cells were disrupted in a French pressure cell and pigmented membranes were obtained by rate-zone sedimentation on sucrose density gradients (*5*); the membranes from strains M21 and M2192, which formed an upper band, were purified further on a second sucrose gradient (*27*). Purified membrane fractions were resuspended in 1 mM Tris (pH 7.5), mixed with glycerol (1:1), and stored at −80 °C.

Electrophoretic Procedures. Preparative LDS−PAGE was performed at 4 °C (*4*) using a thermostated circulating water bath. Membranes were solubilized at LDS/phospholipid (wt/wt) ratios of 2.0−2.5 and run at 50 V through the stacking gel and at 80−100 V overnight in the separating gel. Subsequent steps were also conducted at 4 °C under dim light. Gel bands containing pigment−protein complexes were excised, macerated with a spatula, and homogenized with an electrically driven Teflon and glass homogenizer in ∼4 vol of 10 mM Tris buffer (pH 8.8) containing 0.1% LDS. After 2 to 3 h, acrylamide particles were removed by centrifugation at 10 000 rpm (12000*g*) for 10 min, supernatants were concentrated to ∼1 mL with Amicon Centriprep-30 or Centricon-30 microconcentrators and residual acrylamide was sedimented in a microcentrifuge. The complexes

were concentrated further to ~100 μL, mixed with an equal volume of 80% (v/v) glycerol, and stored at −20 °C.

Ferguson plots (*28*, *29*) (see Supporting Information) were constructed by determining the relative mobilities of the various bands in gels with the concentration of acrylamide plus *N*,*N*′-methylenebis (acrylamide) (%T, w/v) varying between 6 and 20%T, generally in increments of 1.25%T; the proportion of *N*,*N*′-methylenebis(acrylamide) (%C, w/w) was maintained at 2.6%C. Retardation coefficients and free mobilities were obtained from the slopes and the intercepts at zero gel concentration, respectively (see Supporting Information).

Analytical SDS−PAGE was described previously (*5*), using twice concentrated buffer in the separating gel for improved antenna subunit resolution.

For Western blotting as in ref *30*, approximately 15 ng of membranes were electrophoresed according to Schägger and von Jagow (*31*) on a 16.5% gel. Proteins were transferred to nitrocellulose (Hybond ECL, Amersham), the membranes blocked with 5% milk powder, 0.05% Tween-20 in Tris buffered saline. The primary antibody, which recognizes both LH1α and PufX (kindly provided by Prof. R. J. Cogdell), was used at a dilution of 1:5000, reacted with goat-anti rabbit HRP conjugate and revealed using ECL Detection system (Amersham).

Chemical Characterization. BChl and phospholipid concentrations were determined as described previously (*32*). Protein concentrations were estimated (*33*, *34*), using bovine serum albumin as a standard, correcting for interference by LDS, and also by measurements of absorption at 280 nm using an extinction coefficient of $\epsilon_{280\ nm,\ mg/mL} = 5$. Due to different sensitivities of the standard and antenna protein, absolute estimates varied; however, all three methods yielded essentially the same relative values for the series of LH1 complexes.

Spectroscopic Procedures. For low-temperature spectroscopy, samples were suspended in 10 mM Tris (pH 8.8), 0.1% LDS, 60% glycerol, and both absorption and fluorescence spectra were obtained with a Johnson Research Foundation DBS-3 spectrophotometer (University of Pennsylvania, Philadelphia, PA). This instrument was modified to accommodate a DN1704 liquid nitrogen cryostat (Oxford Instruments, Osney Mead, U.K.), and to allow for fluorescence detection at right angles using a HUV 4000B photodiode (EG&G Electrooptics, Salem, MA)). For emission spectra, a J-Y H10-VIR monochromator (Instruments SA, Metuchen, NJ) (12-nm HBW) was used for detection, while absorption and (polarized) fluorescence excitation spectra were measured with a J-Y H20-IR monochromator (4-nm spectral resolution); the detection monochromator was replaced with a 10-nm HBW double cavity interference filter (Omega Optical, Brattleboro, VT) for excitation spectra. Fluorescence polarization measurements were performed with HR sheet polarizers (Polaroid Corporation, Cambridge, MA). Polarization values were expressed as $p = (F_{||} - F_{\perp})/(F_{||} + F_{\perp})$, where $F_{||}$ and $F_{\perp}$ are the relative signals of fluorescence polarized parallel and perpendicular to the direction of the excitation beam, respectively. Because the polarizers do not completely block the perpendicular component of the electric vector (relative transmission $T_{\perp}$ around 900 nm amounting to nearly 10% of that of the parallel component $T_{||}$), measured polarization values (p_{exp}) were lower than those obtainable with ideal polarizers. To correct for this residual transmission, p_{exp} was divided by the value $(T_{||} - T_{\perp})/(T_{||} + T_{\perp})$ at the detection wavelength (~0.85 at 915 nm).

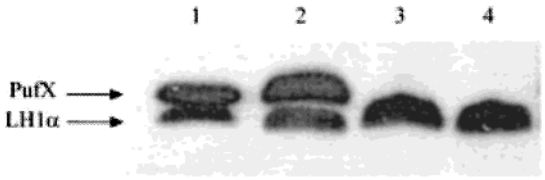

FIGURE 1: Western blot analysis of PufX in membranes from mutants M21 and M2192. The blot was prepared as described in Materials and Methods, and probed with antibodies that recognize both PufX (upper band) and LH1α (lower band). Membrane samples from the wild-type and the PufX⁻ mutant RCLH12X⁻ (*30*) were included as controls. Lane 1, wild-type; lane 2, M21; lane 3, M2192; lane 4, RCLH12X⁻.

RESULTS

Mutant M2192 Lacks the PufX Polypeptide. The Western blot in Figure 1 compares membranes from M21 and M2192, and includes membranes from the wild-type and a previously characterized PufX⁻ mutant (*30*) as controls. The antibodies recognized both LH1α (lower band) and PufX (upper band). As expected, LH1α is present in all samples. The absence of PufX from the M2192 sample is clear, and this experiment shows that M2192, in addition to lacking LH2 and the reaction center, also lacks PufX.

Comparison of Electrophoretic Profiles of Wild-Type and Mutant Strains Lacking Pigment−Protein Complexes. The LDS−PAGE profiles of membranes from *R. sphaeroides* wild-type and mutant strains NF57 and M21 (Figure 2) generally confirmed banding patterns observed previously (*5*). While the majority of the LH1 in M21 was again seen to form multiple bands, the improved resolution of this acrylamide gradient gel revealed a very regular banding pattern, indicative of an oligomeric series of LH1 complexes. NF57 yielded previously unrecognized minor LH2 complexes, with the most prominent (LH2 band 4), comigrating with a distinct wild-type band, as did the oligomeric LH1 series from M21, showing that these aggregates could also be found in the parent strain. This indicates that the core and peripheral antenna complexes were solubilized independently of one another, as would be expected from their existence as distinct ring-like structures (*8*, *11*, *13*), and that the wild-type bands of intermediate migration may represent fortuitously comigrating LH1 and LH2 complexes, rather than in vivo associations, as thought initially (*5*).

While low levels of a similar group of LH1 oligomers were also seen with the LH1-only strain M2192 (Figure 2), most of the protein-associated pigment migrated as an additional band corresponding to a large LH1 aggregate near the top of the gel. These differences in banding patterns between M21 and M2192 were not due to variations in solubilization conditions, since after treatment of membranes from both strains with 3- and 10-fold LDS excesses, their distinct profiles persisted, despite shifting somewhat toward smaller aggregates and some losses in yield, as demonstrated by further pigment loss (not shown). As detailed below, the major, slowly migrating band in strain M2192 is interpreted to represent the fully circular, monomeric (*11*, *35*) LH1 complex that is formed in the absence of PufX, as opposed

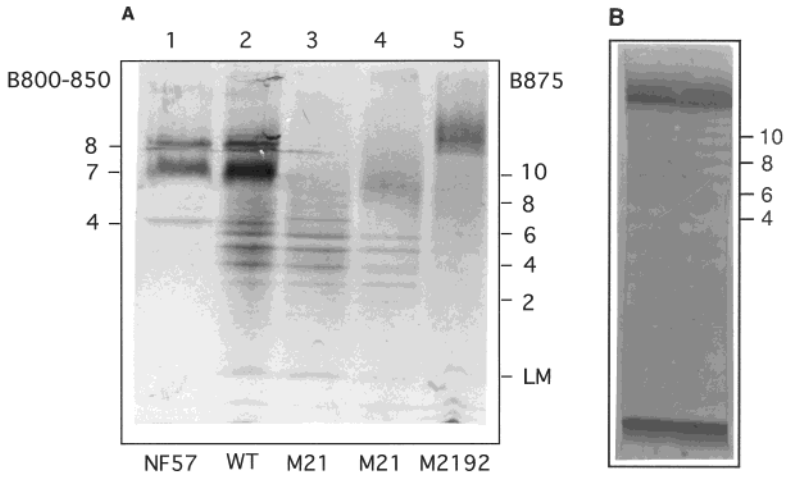

FIGURE 2: LDS−PAGE profiles of membranes from *R. sphaeroides* wild-type and mutant strains. These unstained gels were prepared with a 6−12% (wt/v) acrylamide gradient and run under nondenaturing conditions at 4 °C. (A) Lane 1, strain NF57 (LH1$^-$ reaction center$^-$); lane 2, wild type; lanes 3 and 4, M21 (LH2$^-$) from cells grown under photoheterotrophic and semiaerobic conditions, respectively; lane 5, M2192 (LH2$^-$ reaction center$^-$). Numbers on the left and right designate respective B800−850 (LH2) and B875 (LH1) complexes. LM, reaction center particle, consisting of subunits L and M. LH2−8 was not always reproducible and was not analyzed further. Free pigment at the gel front is not shown. Membranes were purified and their chemical compositions determined as described in Materials and Methods; respective specific BChl (μg of Bchl/mg of protein) and mg of phospholipid/mg of protein values were wild type, 59.6, 0.51; NF57, 58.1, 0.65; M21, photoheterotrophic, 37.1, 0.48; M21, semiaerobic, 26.9, 0.54; M2192, 7.8, 0.80. (B) Lane cut from preparative LDS gel of membranes from strain M2192 (LH2$^-$ reaction center$^-$), showing more distinct bands of intermediate oligomeric states; most pigment is present at the gel front and in the band near the top of the gel, estimated to consist of 13−15 $\alpha\beta$-heterodimers. Numbered bands correspond to those of M21.

Table 1: Specific BChl Content, Oligomeric State, and Absorption and Fluorescence Emission Maxima of LH1 Complexes Isolated by Lithium Dodecyl Sulfate−Polyacrylamide Gel Electrophoresis

gel band	specific BChl[a]	oligomeric state[b]	maxima (nm) at 77 K	
			absorption	fluorescence
1	13.8	1−2	886	902
2	26.7	2−3	889	905
3	39.0	3−4	889	906
4	48.5	4−5	891	908
5	51.2	5−6	891	909
6	47.5	6−7	892	909
7	52.1	7−8	892	908
8	50.7	8−9	891	909
9	36.1	9−10	891	908
10	40.3	10−11	891	908
M21 membranes			890	908

[a] μg of BChl/mg of protein. [b] Number of $\alpha\beta$-heterodimers estimated from analysis of Ferguson plots in which the reaction center LM particle and annular LH1 and LH2 complexes were used as internal standards of known structure.

to the less stable C-shaped dimeric LH1 formed in the presence of PufX (*14*, *35*, *36*).

Composition, Stability, and Size Estimates of LH1 Oligomers. The BChl/protein ratios of eluted LH1 oligomers from M21 (Table 1) were nearly constant (~40−50 μg/mg) for all but the smallest, less abundant complexes, and somewhat lower than reported earlier (*4*), reflecting protein assay differences. Denaturing SDS−PAGE of the LH1 gel bands, equalized on a BChl basis (not shown), revealed that the lower pigment/protein ratios of the smaller aggregates were due to the presence of contaminating polypeptides, comigrating with LH1 bands under nondenaturing conditions, and that the levels and stoichiometries of the α- and β-polypeptides appeared to be similar for all complexes.

An examination of the stability of the isolated M21 complexes in a second LDS−PAGE (Figure 3) revealed that the smaller oligomers migrated largely to their original positions. However, additional bands of both faster and slower mobility appeared, each comigrating with one of the original oligomeric series. Bands 8 to 10 mostly dissociated into a series of smaller species, since the electrophoretic conditions did not favor these higher forms, as is evident in the initial LDS−PAGE separation (Figures 2 and 3). The limited dissociation and reaggregation of oligomers observed upon re-electrophoresis occurred either during recovery from the gel or in the stacking process. The oligomers were found to be less stable at high ionic strength and below neutral pH, which were the conditions used during stacking. The levels of free pigment at the gel front showed that pigment−protein associations in the smallest complexes were generally less stable. The relationship of the oligomer dissociation observed here to that elicited by in vitro alterations in temperature and detergent concentration (*37*), is discussed below.

From an analysis of electrophoretic mobilities as a function of gel concentration, which yielded estimates of free mobility and retardation coefficients (see Supporting Information), the various LH1 oligomers were shown to comprise a series of size isomers, that differ in mass by an essentially fixed amount. To estimate their oligomeric states, the measured retardation coefficients were compared to surface area estimates based on models of detergent solubilized antenna complexes. The intact complexes were considered to represent ellipsoidal cylinders, as assumed for the three internal standards of known structure, viz., the reaction center LM particle and the annular LH1 and LH2 complexes. This was based on the structure of the detergent phase of reaction center crystals determined by neutron diffraction analyses (*38*, *39*), which showed that both lauryl *N*,*N*-dimethylamine-*N*-oxide and OG formed ellipsoidal micellar structures. These had a maximal thickness of 2.5−3.0 nm, and occupied the position of the native phospholipid bilayer, as well as some of the direct contacts normally made with LH1. It is likely

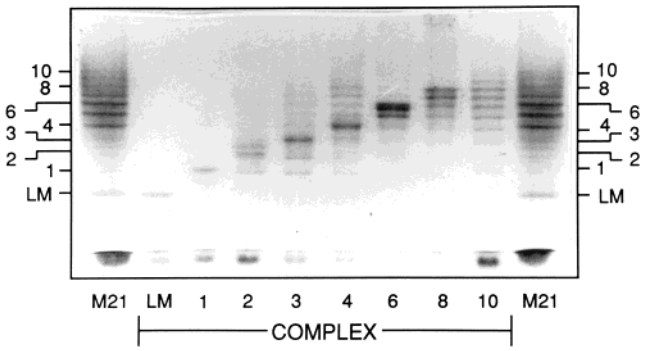

FIGURE 3: Stability of LH1 oligomers isolated from *R. sphaeroides* mutant strain M21 by LDS−PAGE. Membranes from strain M21 (LH2$^-$) grown photoheterotrophically (end lanes) and re-electrophoresis of eluted LH1 bands (inner lanes). The gel (unstained) was prepared with a 7−14% (wt/v) acrylamide gradient and run under nondenaturing conditions at 4 °C. Concentrations of applied LH1 bands were equalized on a BChl basis, except for complex 1 due to limited amounts. Bands 2 to 10 correspond to LH1 complexes with respective estimated aggregation states of 2−3 to 10−11 $\alpha\beta$-heterodimers (Table 1). Cytochrome bands migrated ahead of the LM particle.

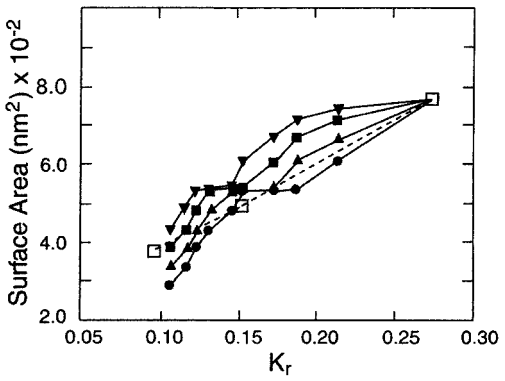

FIGURE 4: Comparison of measured retardation coefficients and modeled surface areas. The large open squares represent the three standard proteins (left to right: reaction center LM particle, LH2 complex (band 4), and the circular LH1 complex of M2192), connected by a dashed line. LH2 band 4 is thought to consist of the annular LH2 complex in which phospholipid has been displaced by LDS, since phospholipid is only associated with the slower migrating band 7 in gels of the wild type (*5*). The four curves (closed circles, triangles, squares, inverted triangles, respectively), connected by solid lines, correspond to bands 2 to 10 with respective assumptions of smallest oligomers as $(\alpha\beta)_2$, $(\alpha\beta)_3$, $(\alpha\beta)_4$, and $(\alpha\beta)_5$, at left, followed by respective consecutive oligomers. The three standards, as well as the LH1 bands, were assumed to bind LDS similarly in a uniform, belt-like 3.0-nm monolayer around the membrane embedded portion of the molecule. The curvature of the LH1 oligomer plots may arise in part from rough surfaces exposed at points where the oligomers have been cut out from the fully formed structure, resulting in underestimates of convex hull surface areas, most notably for the smaller complexes.

that LDS forms a similar detergent belt surrounding the LM subcomplex, which we have also extrapolated to models of LDS-solubilized LH2 and LH1 fractions (see Supporting Information).

For estimating the convex hulls enclosing partially complete LH1 rings, the requisite number of degrees from the ring (22.5° per $\alpha\beta$ unit) were taken before decorating it with detergent and calculating the surface area of the hull. The results of these calculations (Figure 4), in which ellipsoidal micellar structures with a thickness of 3.0 nm in the normal position of the bilayer were assumed, show that for LH1 complexes 2−10, the curves corresponding to the oligomeric series running from $(\alpha\beta)_{2-10}$ and $(\alpha\beta)_{3-11}$ fit most closely with the standards. These complexes differ in size (Table 1) by a fundamental structural unit, suggested to consist of an $\alpha\beta$-heterodimer. A fully circular pigment−protein array, in which the finite maximum aggregation state would be imposed, could explain the distinct, slowly migrating major gel band obtained with membranes from strain M2192 (Figure 2B), which gave an estimate of ∼13−15 $\alpha\beta$-heterodimers, with dimensions close to those of the *Rs. rubrum* complex (*13*).

Optical Properties of LH1 Oligomers. Absorption and fluorescence emission spectra of the isolated complexes at 77 K showed 6−7 nm red shifts in the Q_y band as the aggregation state increased from ∼2 to ∼6−7 (Figure 5), and essentially constant Stokes shifts of 16−18 nm (Table 1). These shifts were accompanied by a slight reduction in the bandwidths from ∼35 to ∼32 nm for absorption and from ∼35 to ∼30 nm for emission spectra; in intact membranes, absorption and emission bands both had a width of ∼30 nm. The fluorescence excitation spectra for the various oligomers were red shifted by 1−2 nm relative to the respective absorption spectra. This was not an experimental artifact, since absorption and excitation spectra were obtained with the same excitation source and the lack of alignment was not observed with intact M21 membranes. Instead, these observations are attributed to spectral heterogeneity, in which fluorescence in the long-wavelength tail of the emission band would primarily originate from a more red-shifted subpopulation of complexes. Moreover, emission maxima were blue shifted by 1−2 nm upon selective excitation in the blue wing of the absorption band (865−875 nm), relative to those

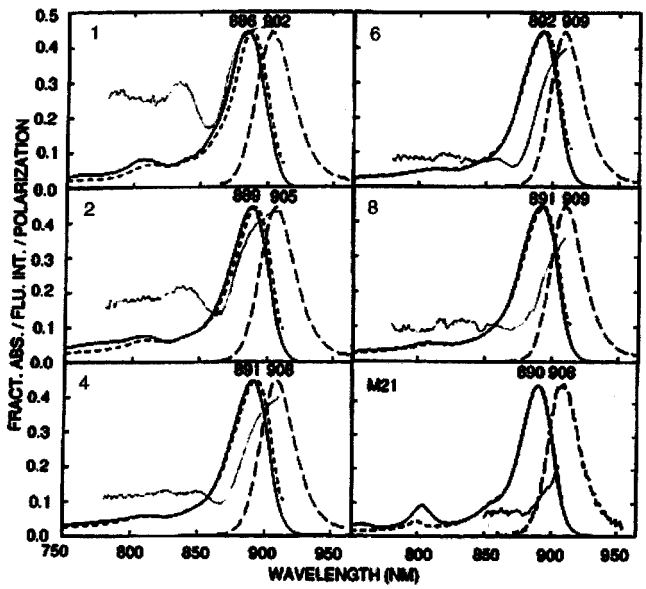

FIGURE 5: Optical properties of LH1 oligomers from *R. sphaeroides* strain M21 at 77 K. Fractional absorption (1-T) spectra, (—); emission spectra, (− −) (excitation at 590 nm); excitation spectra, (- - -); fluorescence polarization, (···). Fluorescence excitation and polarized excitation spectra were detected with a 935-nm band-pass filter; polarization values were corrected as described in the text. Gel band numbers of isolated complexes and absorption and fluorescence emission maxima (Table 1) are indicated. Some contamination by the P800 band of the reaction center is seen in the smaller complexes. It is possible that the spectra for band 8 were influenced by some dissociation into smaller oligomers, as observed upon re-electrophoresis (Figure 3).

obtained upon nonselective Q_x-band excitation (not shown). Since the heterogeneity in oligomer size observed upon re-electrophoresis (Figure 3) was limited mainly to the larger complexes, this would not be expected to make a major contribution to these emission band inhomogeneities. Thus, a more likely possibility is that they arise from inhomogeneities in site energies, initially proposed as an explanation for the multiphasic fluorescence decay kinetics of the core antenna (*40*). Numerical simulations of the optical properties described here (*20*) suggested that small red shifts of the excitation spectrum relative to the absorption band can indeed be well explained by selective excitation of a nonrandom subfraction of a collection of LH1 BChl arrays, without the need to invoke a heterogeneity in size.

Fluorescence polarization spectra of the larger complexes were similar to that of the membrane-bound LH1 complex with low polarization values (p) of ~0.1 at the blue side of the Q_y band and increases over the red wing (Figure 5). With decreasing oligomer size, the rise in polarization gradually shifted toward the blue side of the absorption band; the polarization spectrum for the smallest complex reached a maximum value of ~0.42 near the center of the band. This value is essentially equal to that obtained with BChl in cyclohexanol on the same apparatus and is therefore consistent with parallel absorption and emission dipoles. The wavelength-dependence of fluorescence polarization for this complex resembled that of the B820 subunit form of the LH1 complex (*41*), originally isolated by Loach and collaborators (*42*, *43*), and thought to represent a dimeric BChl ($\alpha_1\beta_1$-$BChl_2$) arrangement (*44*, *45*−*47*).

Apparent LH1 oligomers of different sizes have also been observed in *R. sphaeroides* mutants in which the *puf*A gene was modified to produce truncated C-termini in the LH1α polypeptide (*21*). These mutants showed lowered LH1/reaction center ratios, accompanied by progressive blue shifts in LH1 absorbance maxima (Figure 6); e.g., strain RCLH+13 with a 13-amino acid truncation gave rise to a 5-nm blue shift and a decrease in size from ~30 to 10 mol of LH1 BChl/mol reaction center in a detergent-solubilized core complex. In contrast, in strain RCLH+21 with five amino acids truncated, the size was reduced to 20 BChls per reaction center and the position of the absorption band was unchanged. The lowered LH1/RC stoichiometries suggested their LH1 complexes have reduced sizes and are incapable of surrounding the reaction center. This complementary approach provided an opportunity to obtain data on complexes in their native membrane environments, free from detergent. As with M21, these mutants all contain PufX (*21*). Fluorescence polarization measurements performed on the isolated membranes (Figure 6) revealed a relationship between the absorption blue shifts and wavelength dependence of fluorescence polarization similar to that observed with the LDS complexes. This correspondence of optical properties supports the conclusion that the results obtained for the detergent-solubilized LH1 complexes are indeed related to their oligomeric state and are not an artifact caused by removal from the membrane environment or denaturation by detergent.

Circular dichroism spectra (not shown) obtained at room temperature with several of the LH1 oligomers (Visschers, R. W., and Westerhuis, W. H. J., unpublished) showed positive values around 895 nm, accompanied by a broad

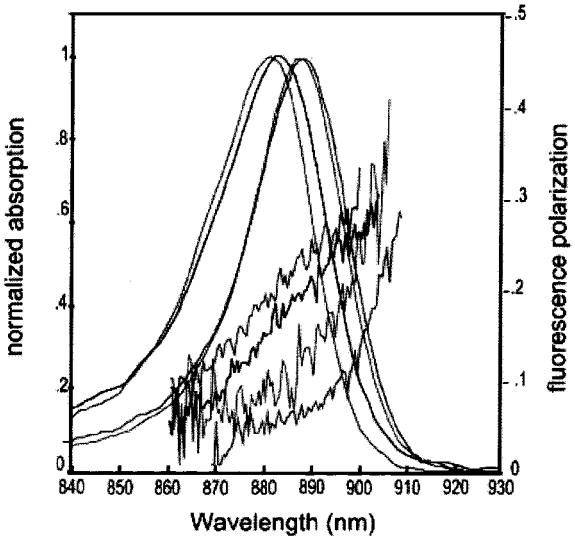

FIGURE 6: Optical properties at 77 K of intracytoplasmic membranes from *R. sphaeroides* strains forming LH1 complexes with truncated C-termini in their LH1α polypeptides (*21*). Left to right: Strain RCLH+12 with a 14-amino acid truncation; strain RCLH+13 with a 13-amino acid truncation; strain RCLH+21 with a 5-amino acid truncation; RCLH12, RC/LH1 control strain. Absorption maxima were at 881, 883, 889, and 888 nm, respectively (*21*). The higher noise levels in the wavelength dependence of the fluorescence polarization arise from the presence of reaction centers in these strains which reduced their fluorescence yields.

negative band between ~830 and 880 nm, characteristic of the isolated *R. sphaeroides* LH1 complex (*48*). While the position of the negative band in complex 10 was centered around 860 nm, as in the native complex (*49*), it was blue shifted by up to 10 nm in the smaller oligomers, in which the CD was somewhat less intense. Overall, these results indicate that in the various oligomers, little alteration has occurred in the relative orientations of their LH1 BChls, or in the extent of coupling between them.

Ultrastructural Analysis of Photosynthetic Units in R. sphaeroides M21. As a means of relating the isolated pigment−protein complexes to the intramembrane core particle structures from which they arise, freeze-fracture electron microscopy was performed on whole cells of M21, a strain that forms elongated tubular membranes, rather than the vesicular ICM present in LH2 containing strains (*5*, *50*). Freeze-fracture replicas showed a striking pattern of closely packed, dimeric particles with dimensions of ~100 × 200 Å that were highly ordered and arrayed helically along the longitudinal axes of the tubules (Figure 7). Since these particles apparently contain photosynthetic unit cores, they may represent a dimer of reaction centers with surrounding LH1 assemblies. Supporting this possibility is a recent electron microscopy projection map of negatively stained tubular membranes from another $LH2^-$ *R. sphaeroides* strain (*14*), in which apparent supercomplexes were visualized. These were thought to consist of two C-shaped LH1 arrays surrounding a dimeric reaction center, with the remaining positive density attributed tentatively to one cytochrome bc_1 complex (see, however, ref *52*).

DISCUSSION

The Various LH1 Bands Represent a Regular Oligomeric Series. The regularity and discrete nature of the ladder of

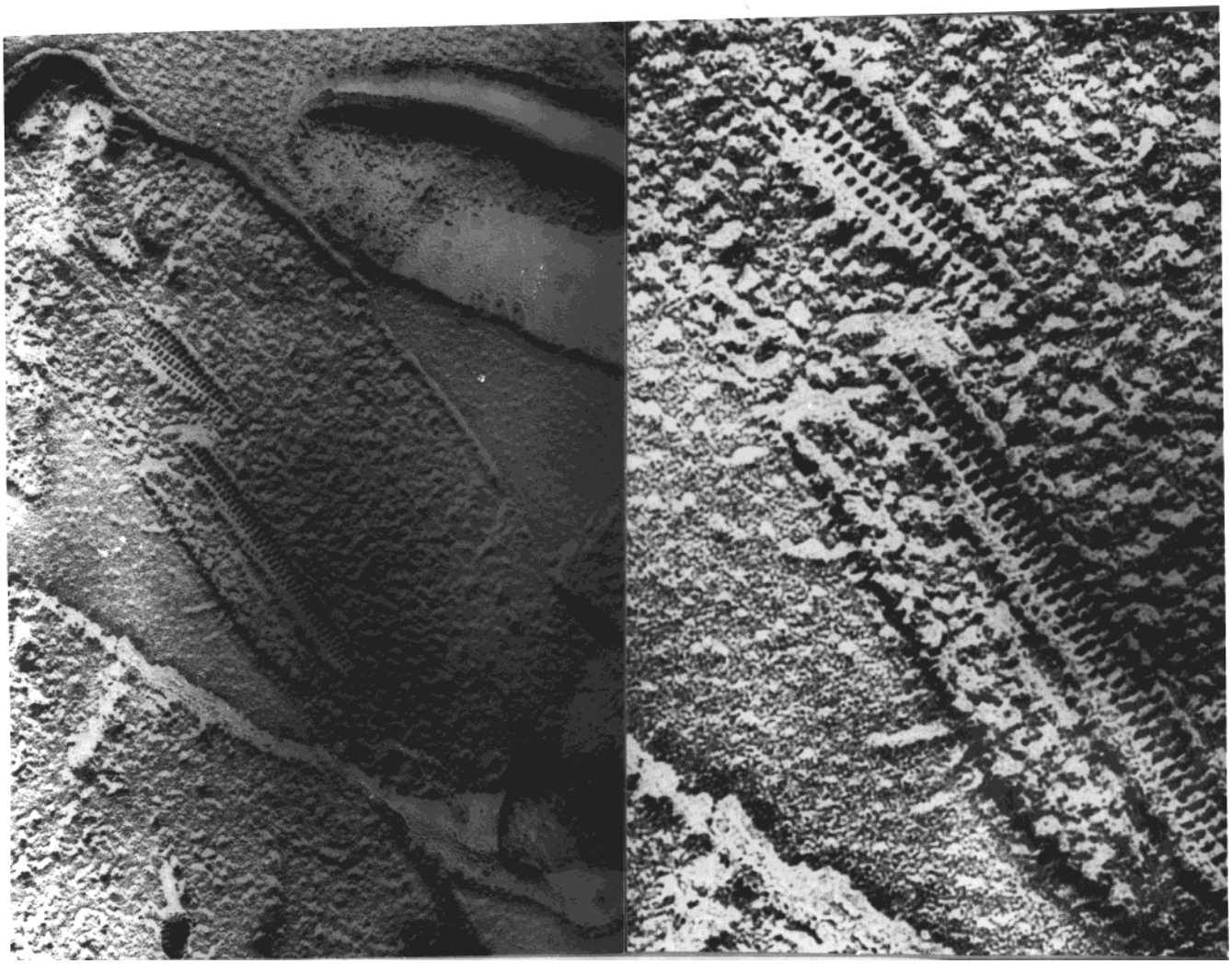

FIGURE 7: Electron micrograph of freeze-fracture replica of *R. sphaeroides* strain M21 cells. Left, whole cells, 52000×. Right, elongated tubular membrane structures, 119000×. Cells were frozen in a Balzers model QFD 020 liquid propane cryo-jet device, freeze-etched, shadowed with platinum and examined in a JEOL JEM-100 CXII electron microscope as described previously (*51*). Diameter of tubules ≈650 Å.

LH1 bands in LDS−PAGE, taken together with their compositional and spectral integrity and estimated sizes, show that these complexes consists of an oligomeric series, differing in size by the M_r of their basic $\alpha_1\beta_1BChl_2$ structural unit. The separation of the individual LH1 bands in strain M21 by nearly equal increments, and their total, reproducible number of 10, further confirms that this heterodimeric $\alpha_1\beta_1$-$BChl_2$ structure is the largest possible unit that could be added during oligomerization. This is also the composition of the B820 subunit of LH1 isolated by OG treatment that can be reconstituted into a fully formed LH1 complex (*42*−*44*).

In a recent study of the oligomerization of the *Rs. rubrum* LH1 (B873) complex during in vitro reconstitution of the B820 to the full B873 ring, either by OG-mediated transitions or incremental temperature changes, several intermediate oligomeric forms were transiently observed (*37*). One of these had an absorption maximum near 850 nm, representing a putative $\alpha_2\beta_2BChl_4$ structure, while a variety of oligomers with slightly blue-shifted absorption spectra also appeared that apparently exist as incomplete rings, missing a few $\alpha_1\beta_1$-$BChl_2$ units. This was proposed to reflect an equilibrium of different sized aggregates, with reassociation of the B820 subunit to the full B873 ring occurring through a moderately cooperative assembly process proceeding via these intermediate oligomeric states.

While the existence of partially formed spectral intermediates during reconstitution of the B820 subunit to the full B873 complex had been recognized previously by others (*43*, *53*, *54*), their transient nature differs from the more stable oligomeric complexes isolated in the present study. Although some dissociation and reaggregation of oligomers was observed upon re-electrophoresis (Figure 3), this can be avoided by obtaining spectra directly from gel slices, as was done initially (*4*). Since such an oligomeric series is useful for the photophysical analysis of the role of heterodimer associations in governing the optical properties of LH complexes, it is necessary to rely upon LDS treatment and the electrophoretic procedures described here for their preparation. In this connection, the recent reconstitution of the *R. sphaeroides* LH1 antenna with Ni-substituted BChl provides an alternative approach for the analysis of unit size and excited-state properties of a series of LH1 oligomers (*55*).

Interpretation of the Optical Properties of LH1 Oligomers. These studies have demonstrated that it is possible to isolate different aggregation states of the basic LH1 $\alpha\beta$-heterodimer

complex with a progression of red-shifted absorption and fluorescence emission maxima and fluorescence polarization properties. The correlation of these differences with aggregate size shows that LDS−PAGE analysis represents a powerful tool for examining the role of interunit interactions in determining the final optical properties of the fully assembled antenna. The relationship observed between oligomer size and spectroscopic properties was not due to selective pigment loss, since the BChl/antenna protein ratio appeared to be similar, even in the smaller complexes.

The optical properties of the LH1 oligomeric series, solubilized from the membranes of strain M21, have been described in part by a model in which the LH1 BChls are organized in a curvilinear array of excitonically coupled dimeric chromophores (*20*). Excitonic coupling provided the simplest explanation for the oligomeric state-dependent absorption and emission red shifts. However, spectral simulations demonstrated that to account satisfactorily for the fluorescence polarization differences across the Q_y band, it was also necessary to assume an inhomogeneous distribution of BChl site energies (*56*), thought to reflect small, random differences in local pigment environments (*40*). In this model, the anisotropic long-wavelength component, designated originally as B896, is proposed to arise principally from low energy excitonic transitions, rather than from a distinct subantenna species as proposed initially (*57*). The relative contribution of this red-wing component increased as the cluster size of the arrays was decreased, as reflected in the fluorescence polarization rise across the Q_y band. In the smallest complex, this rise is similar to that of the LH1 B820 subunit (*41*), which was proposed to originate from a BChl dimer with two excitonically coupled BChls, having a parallel configuration and an angle between the Q_y transition dipoles of ∼30°. A pronounced dip in the wavelength-dependence of the fluorescence polarization on the blue side of the Q_y band, attributed to a high-energy exciton component, was observed here, especially in the smaller LH1 aggregates (Figure 5).

The asymmetric organization of the putative dimeric LH1-reaction center complexes has been suggested (*14*, *35*) to provide a possible structural basis for the anisotropic long-wavelength B896 component. Accordingly, LH1 subunits next to an opening in the ring were proposed to have different absorption characteristics, acting as privileged sites for energy transfer to the reaction center (*14*). However, when numerical simulation of spectral inhomogeneity was applied to sections of a circular model (*20*), removal of a single unit from a full circle resulted in a gain in oscillator strength on the blue side of the absorption band which became slightly more asymmetric. Moreover, excitons associated with these edge pigments were, on average, less red shifted, as shown by the blue-shifted spectra of LH1 aggregates of reduced size (Figure 5), with their higher proportion of edge chromophores. Thus, in strains lacking PufX in which the enlarged LH1 circle is closed (*11*), absorption spectra were more symmetric and red shifted by ∼4 nm (*58*).

The Origin of the LH1 Oligomers and their Relationship to the Supramolecular Organization of Photosynthetic Units. What is the origin of these multiple oligomeric states for LH1, and why have they not been observed for LH2? Pugh et al. (*30*) have proposed a modular assembly and structure for LH1, in which the basic unit for assembly is an LH1$\alpha_1\beta_1$-$BChl_2$ complex. Each $\alpha_1\beta_1BChl_2$ unit is stabilized by the network of hydrogen bonds, as shown by the resonance Raman studies of site-directed mutants of LH1 (*59*−*61*). These data show that there are four hydrogen bonds "internal" to the B820 unit which provide a significant driving force to stabilize this complex (*62*). In contrast, the analogous hydrogen bonding arrangement in LH2 from *R. sphaeroides* and *R. acidophila* is not of this type (*8*, *63*). One consequence of the stability of the $\alpha_1\beta_1BChl_2$ unit is that it can be serially removed from an LH1 oligomer, leaving a number of LH1 complexes, each differing from another by one $\alpha_1\beta_1BChl_2$ unit, as demonstrated here.

In the LDS−PAGE profiles of both strains M21 and M2192, the smaller bands are proposed to represent fragments of such an array, while the largest complex from the latter strain is attributed to a closed circular structure. The pigment distribution in strain M2192 is similar to that observed with LH1 from the related bacteria *Rs. rubrum* (Westerhuis, W. H. J., and Niederman, R. A., unpublished) and *Rs. centenum* (Sturgis, J. N., unpublished). We believe that this arises from the absence of PufX, leading to the formation of closed annular LH1 complexes, at least in the case of *Rs. rubrum* (*13*), for which an $(\alpha\beta)_{16}$ structure was observed. These closed annular structures have been isolated in a monomeric state in the absence of PufX (*35*), while in the presence of PufX, LH1 is thought to form two C-shaped structures surrounding a dimeric reaction center (*14*, *36*).

As noted above, partially circular LH1 complexes are also thought to be formed by the *R. sphaeroides* strains with truncated C-termini in their LH1α polypeptides (*21*). Although they remained in functional contact with the reaction center, their absorption and fluorescence polarization spectra (Figure 6) showed the same trend as those of the LH1 oligomers isolated by LDS−PAGE, suggesting further that these optical properties are a function of aggregation state.

The appearance of the intramembrane particles observed in freeze-fracture replicas (Figure 7) suggests that LH1-reaction center complexes are organized into dimeric structures in M21 as proposed Jungas et al. (*14*) for another LH2-minus strain. It is important to note that these freeze-fracture data provide direct evidence for long-range organization of membrane components in an LH2-minus mutant, independent from the conclusions drawn from the image analysis data (*14*) and linear dichroism studies (*19*).

Role for PufX in the Assembly of Photosynthetic Unit Cores. It is noteworthy that current models (*14*, *17*, *36*) for the structure of the core assemblies in *R. sphaeroides* also suggest a specific role for the PufX protein. This protein, which is encoded by the *puf*X gene, located in the *puf*QBALMX operon, and associated with isolated LH1-reaction center core structures (*64*), is required for photosynthetic growth in both *R. sphaeroides* (*65*) and *R. capsulatus* (*66*). Recently, it has been shown that PufX inhibits reconstitution of the B820 complex (*67*) by associating with the LH1 α polypeptide via the core PufX segment containing its putative transmembrane α-helix (*68*). In addition, interaction studies in detergent-solubilized complexes (*30*) showed that PufX binds best to LH1-reaction center complexes, followed by LH1 alone and reaction center alone.

As noted above, PufX is also essential for promoting long-range order in LH1-reaction center complexes of *R. sphaeroi-*

des (*19*). Our demonstration that ordered arrays of particles can be seen following freeze-fracture of M21 membranes is consistent with the presence of PufX in M21, as confirmed by immunoblotting (Figure 1). Singlet−singlet annihilation data indicated that M21 had a greater tendency to contain large energy transfer domains than the PufX$^-$ strain M2192 (*69*). While this was attributed to the absence of reaction centers in M2192 (*23*), it is also possible that PufX played a role in association of LH1-reaction center domains, as shown later by linear dichroism (*19*). Similarly, differences in fluorescence anisotropy decay between these strains could have arisen from the absence of PufX from M2192 (*70*).

Finally, it should be noted that both the arrangement and presence of supercomplexes in *R. sphaeroides* remain a matter of debate (*52*), since the kinetic behavior attributed in whole cells to electron flow within supercomplexes, has not been demonstrated in chromatophores. This has been explained by a heterogeneity in the distribution of redox components among a vesicle population in which cytochrome c_2 freely diffuses, a possibility that could arise from perturbations of supercomplex structure during chromatophore preparation, permitting unimpeded diffusion of cytochrome c_2 within the intravesicular space. An additional consideration is the different experimental material used in the various studies. For example, in recent work on tubular membranes from LH2$^-$ mutants (*14*, *19*), these strains were prepared with plasmid-borne copies of the *puf* operon expressed in a *puf* deletion background. This works well for manipulations of the *puf* operon itself, but it is reasonable to assume that reaction center/cytochrome bc_1 stoichiometry could be perturbed in such strains, due to a plasmid copy number effect. This could easily have a bearing on kinetic, spectroscopic, and structural studies of supercomplexes in these strains. The significance of the freeze-fracture data reported in this work is that mutant M21 contains a simple point mutation of the *puc* operon, and there is less likelihood of complicating factors regarding reaction center:cytochrome bc_1 stoichiometry. The fact that organized structures can be observed in membranes from M21 is therefore of considerable importance. Clearly, much additional effort will be necessary before a more complete picture of the supramolecular organization of the bacterial photosynthetic unit will be able to emerge.

SUPPORTING INFORMATION AVAILABLE

Ultrastructural characterization of strains used in this study, and further details on the estimation of oligomer sizes by analysis of electrophoretic mobility. This material is available free of charge via the Internet at http://pubs.acs.org.

REFERENCES

1. van Grondelle R., Dekker, J. P., Gillbro, T., and Sundström, V. (1994) *Biochim. Biophys. Acta 1187*, 1−65.
2. Theiler, R., Suter, F., Zuber, H., and Cogdell, R. J. (1984) *FEBS Lett. 175*, 231−237.
3. Theiler, R., Suter, F., Pennoyer, J. D., Zuber, H., and Niederman, R. A. (1985) *FEBS Lett. 184*, 231−236.
4. Broglie, R. M., Hunter, C. N., Delepelaire, P., Niederman, R. A., Chua, N.-H., and Clayton, R. K. (1980) *Proc. Natl. Acad. Sci. U.S.A. 77*, 87−91.
5. Hunter, C. N., Pennoyer, J. D., Sturgis, J. N., Farrelly, D., and Niederman, R. A. (1988) *Biochemistry 27*, 3459−3467.
6. Evans, M. B., Cogdell, R. J., and Britton, G. (1988) *Biochim. Biophys. Acta 935*, 292−298.
7. Zuber, H. (1990) in *Molecular Biology of Membrane-Bound Complexes in Phototrophic Bacteria* (Drews, G., and Dawes, E. A., Eds.) pp 161−180, Plenum, New York.
8. McDermott, G., Prince, S. M., Freer, A. A., Hawthornthwaite-Lawless, A. M., Papiz, M. Z., Cogdell, R. J., and Isaacs, N. W. (1995) *Nature 374*, 517−521.
9. Vos, M., van Grondelle, R., van der Kooij, F. W., van de Poll, D., Amesz, J., and Duysens, L. N. M. (1986) *Biochim. Biophys. Acta 850*, 501−512.
10. Koepke, J., Hu, X., Muenke, C., Schulten, K., and Michel, H. (1996) *Structure 4*, 581−597.
11. Walz, T., Jamieson, S. J., Bowers, C. M., Bullough, P. A., and Hunter, C. N. (1998) *J. Mol. Biol. 282*, 833−845.
12. Scheuring, S., Reiss-Husson, F., Engel, A, Rigaud, J.-L., and Ranck, J.-L. (2001) *EMBO J. 20*, 3029−35.
13. Karrasch, S., Bullough, P. A., and Ghosh, R. (1995) *EMBO J. 14*, 631−638.
14. Jungas, C., Ranck, J.-L., Rigaud, J.-L., Joliot, P., and Verméglio, A. (1999) *EMBO J. 18*, 534−542.
15. Conroy, M. J., Westerhuis, W. H. J., Parkes-Loach, P. S., Loach, P. A., Hunter, C. N., and Williamson, M. P. J. (2000) *J. Mol. Biol. 298*, 83−94.
16. Sorgen, P. L., Cahill, S. M., Krueger-Koplin, R. D., Krueger-Koplin, S. T., Schenck, C. C., and Girvin, M. E. (2002) *Biochemistry 41*, 31−41.
17. Cogdell, R. J., Fyfe, P. K., Barrett, S. J., Prince, S., Freer, A. A., Isaacs, N. W., and Hunter, C. N. (1996) *Photosynth. Res. 48*, 55−63.
18. McGlynn, P., Hunter, C. N., and Jones, M. R. (1994) *FEBS Lett. 349*, 349−353
19. Frese, R. N., Olsen, J. D., Branvall, R., Westerhuis, W. H., Hunter, C. N., and van Grondelle, R. (2000) *Proc. Natl. Acad. Sci. U.S.A. 97*, 5197−5202.
20. Westerhuis, W. H. J., Hunter, C. N., van Grondelle, R., and Niederman, R. A. (1999) *J. Phys. Chem. B* 103, 7733−7742.
21. McGlynn, P., Westerhuis, W. H. J., Jones, M. R., and Hunter, C. N. (1996) *J. Biol. Chem. 271*, 3285−3292.
22. Ashby, M., Coomber, S. A., and Hunter, C. N. (1987) *FEBS Lett. 213*, 245−248.
23. Hunter, C. N., van Grondelle, R., and van Dorssen, R. J. (1989) *Biochim. Biophys. Acta 973*, 383−389.
24. Hunter, C. N., and van Grondelle, R. (1988) in *Photosynthetic Light-Harvesting Systems* (Scheer, H., and Schneider, P., Eds.) pp 247−260, Walter de Gruyter, New York.
25. Hunter, C. N., and Turner, G. (1988) *J. Gen. Microbiol. 134*, 1471−1480.
26. Olivera, L. M., and Niederman, R. A. (1993) *Biochemistry 32*, 858−866.
27. Reilly, P. A., and Niederman, R. A. (1986) *J. Bacteriol. 167*, 153−159.
28. Ferguson, K. A. (1964) *Metabolism 13*, 985−1002.
29. Rodbard, D., and Chrambach, A. (1971) *Anal. Biochem. 40*, 95−134.
30. Pugh, R. J., McGlynn, P., Jones, M. R., and Hunter, C. N. (1998) *Biochim. Biophys. Acta 1366*, 301−316.
31. Schägger, H., and von Jagow, G. (1987) *Anal. Biochem. 166*, 368−379.
32. Collins, M. L. P., and Niederman, R. A. (1976) *J. Bacteriol. 126*, 1316−1325.
33. Markwell M. A. K., Haas, S. M., Bieber, L. L., and Tolbert, N. E. (1978) *Anal. Biochem. 87*, 206−212.
34. Bradford, M. M. (1976) *Anal. Biochem. 72*, 248−254.
35. Francia, F., Wang, J., Venturoli, G., Melandri, B. A., Barz, W. P., and Oesterhelt, D. (1999) *Biochemistry 38*, 6834−6845.
36. Westerhuis, W. H. J., Vos, M., van Grondelle, R., Amesz, J., and Niederman, R. A. (1998) *Biochim. Biophys. Acta 1366*, 317−329.
37. Pandit, A., Visschers, R. W., van Stokkum, I. H., Kraayenhof, R., and van Grondelle, R. (2001) *Biochemistry 40*, 12913−12924.
38. Roth, M., Lewitt-Bentley, A., Michel, H., Deisenhofer, J., Huber, R., and Oesterhelt D. (1989) *Nature 340*, 659−662.
39. Roth, M., Arnoux, B., Ducruix, A., and Reiss-Husson, F. (1991) *Biochemistry 30*, 9403−9413.
40. Timpmann, K., Freiberg, A., and Godik, V. I. (1991) *Chem. Phys. Lett. 182*, 617−622.
41. Visschers, R. W., Chang, M. C., van Mourik, F., Parkes-Loach, P. S., Heller, B. A., Loach, P. A., and van Grondelle, R. (1991) *Biochemistry 30*, 5734−5742.
42. Loach, P. A., Parkes, P. S., Miller, J. F., Hinchigeri, S., and Callahan, P. M. (1985) in *Molecular Biology of the Photosynthetic*

Apparatus (Steinbach, K. E., Bonitz, S., Arntzen, C. J., Bogorad, L., Eds.) pp 197−209, Cold Spring Harbor Laboratory, Cold Spring Harbor, NY.
43. Miller, J. F., Hinchigeri, S. B., Parkes-Loach, P. S., Callahan, P. M., Sprinkle, J. R., Riccobono, J. R., and Loach, P. A. (1987) *Biochemistry 26*, 5055−5062.
44. Chang, M. C., Callahan, P. M., Parkes-Loach, P. S., Cotton, T., and Loach, P. A. (1990) *Biochemistry 29*, 421−429.
45. van Mourik, F., van der Oord, J. R., Visscher, K. J., Parkes-Loach, P. S., Loach, P. A., Visschers, R. W., and van Grondelle, R. (1991) *Biochim. Biophys Acta 1059*, 111−119.
46. Visschers, R. W., van Mourik, F., Monshouwer, R., and van Grondelle, R. (1993) *Biochim. Biophys Acta 1141*, 238−244.
47. van Mourik, F., Corten, E. P. M., van Stokkum, I. H. M., Visschers, R. W., Loach, P. A., Kraayenhof, R., and van Grondelle, R. (1992) in *Research in Photosynthesis*, Vol. 1 (Murata, N., Ed.) pp 101−104, Kluwer, Boston.
48. Bolt, J. D., Hunter, C. N., Niederman, R. A., and Sauer, K. (1981) *Photochem. Photobiol. 34*, 653−656.
49. Sturgis, J. N., and Niederman, R. A. (1990) *Photosynth. Res. 23*, 241−248.
50. Sturgis, J. N., Hunter, C. N., and Niederman, R. A. (1990) in *Molecular Biology of Membrane-Bound Complexes in Phototrophic Bacteria* (Drews, G., and Dawes, E. A., Eds.) pp 219−226, Plenum, New York.
51. Theiler, R., and Niederman, R. A. (1991) *J. Biol. Chem*. *266*, 23157−23162.
52. Crofts, A. R. (2000) *Trends Microbiol. 8*, 105−106.
53. Ghosh, R., Hauser, H., and Bachofen, R. (1988) *Biochemistry 27*, 1004−1014.
54. Beekman, L. M. P., Steffen, M., van Stokkum, I. H. M., Olsen, J. D., Hunter, C. N., Boxer, S. G., and van Grondelle, R. (1997) *J. Phys. Chem. B 101*, 7284−7292.
55. Fiedor, L., Leupold, D., Teuchner, K., Voigt, B., Hunter, C. N., Scherz, A., and Scheer, H. (2001) *Biochemistry 40*, 3737−3747.
56. van Mourik, F., Visschers, R. W., and van Grondelle, R. (1992) *Chem. Phys. Lett. 193*, 1−7.
57. Kramer, H. J. M., Pennoyer, J. D., van Grondelle, R., Westerhuis, W. H. J., Niederman, R. A., and Amesz, J. (1984) *Biochim. Biophys. Acta 767*, 335−344.
58. Westerhuis, W. H. J., Farchaus, J. W., and Niederman, R. A. (1993) *Photochem. Photobiol. 58*, 460−463.
59. Olsen, J. D., Sockalingum, G. D., Robert, B., and Hunter, C. N. (1994) *Proc Natl. Acad. Sci. U.S.A. 91*, 7124−7128.
60. Olsen, J. D., Sturgis, J. N., Westerhuis, W. H. J., Hunter, C. N., and Robert, B. (1997) *Biochemistry 36*, 12625−12632.
61. Sturgis, J. N., Olsen, J. D., Robert, B., and Hunter, C. N. (1997) *Biochemistry 36*, 2772−2778.
62. Davis, C. M., Bustamante, P. L., Todd, J. B., Parkes-Loach, P. S., McGlynn, P., Olsen, J. D., McMaster, L., Hunter, C. N., and Loach, P. A. (1997) *Biochemistry 36*, 3671−3679.
63. Fowler, G. J. S., Sockalingum, G. D., Robert, B., and Hunter, C. N. (1994) *Biochem. J. 299*, 695−700.
64. Farchaus, J. W., Barz, W. P., Grünberg, H., and Oesterhelt D. (1992) *EMBO J. 11*, 2779−2788.
65. Farchaus, J. W., Gruenberg, H., and Oesterhelt, D. (1990) *J. Bacteriol. 172*, 977−985.
66. Lilburn, T. G., Haith, C. E., Prince, R. C., and Beatty, J. T. (1992) *Biochim. Biophys. Acta 1100*, 160−170.
67. Recchia, P. A., Davis, C. M., Lilburn, T. G., Beatty, J. T., Parkes-Loach, P. S., Hunter, C. N., and Loach, P. A. (1998) *Biochemistry 37*, 11055−11063.
68. Parkes-Loach, P. S., Law, C. J., Recchia, P. A., Kehoe, J., Nehrlich, S., Chen, J., and Loach, P. A. (2001) *Biochemistry 40*, 5593−5601.
69. Vos, M., van Dorssen, R. J., Amesz, J., van Grondelle, R., and Hunter, C. N. (1988) *Biochim. Biophys. Acta 933*, 132−140.
70. Hunter C. N., Bergström, H., van Grondelle R., and Sundström, V. (1990) *Biochemistry 29*, 3203−3207.

BI011663B